

Late transition-metal oxides with infinite-layer structure: Nickelates versus cuprates

Frank Lechermann

I. Institut für Theoretische Physik, Universität Hamburg, Jungiusstr. 9, 20355 Hamburg, Germany

The correlated electronic structure of the infinite-layer compounds NdNiO_2 and SrCuO_2 at stoichiometry and with finite hole doping is compared. Key differences are elucidated from an advanced first-principles many-body perspective. Contrary to the charge-transfer insulating cuprate, the self-doped nickelate remains non-insulating even for large interaction strength, though the $\text{Ni-}d_{x^2-y^2}$ spectral weight is also gapped in that limit. Hybridization between $\text{Ni}(3d)$ and $\text{Nd}(5d)$ is crucial for the appearance of the self-doping band. Upon realistic hole doping, $\text{Sr}_{1-y}\text{CuO}_2$ shows the expected mixed oxygen- $\text{Cu-}d_{x^2-y^2}$ (Zhang-Rice) states at low-energy. In the case of $\text{Nd}_{1-x}\text{Sr}_x\text{NiO}_2$, the self-doping band is shifted to higher energies and a doping-dependent d_{z^2} -versus- $d_{x^2-y^2}$ competition on Ni is revealed. The absence of prominent Zhang-Rice physics in infinite-layer nickelates might be relevant to understand the notable difference in the superconducting T_c 's.

Introduction.— The competing energy scales of charge-transfer and on-site Coulomb kind are important for various properties of transition-metal (TM) oxides¹, including high-temperature superconductivity in doped layered cuprates². Recently, Li *et al.* reported superconductivity up to $T_c = 15$ K in the infinite-layer (IL) nickelate NdNiO_2 with hole doping³. It was achieved by thin-film generation via soft-chemistry topotactic reduction on a SrTiO_3 substrate. Albeit these results are debated in view of the underlying structural details^{4,5}, this first successful finding of a respectable superconducting regime in conjunction with a layered-cuprate analogon from the nickelate family is remarkable^{6–17}.

The IL architecture usually refers to perovskite(-like) ABO_n crystals in which the apical oxygens are missing, hence BO_2 square lattices are stacked with separating \mathcal{A} layers. Transition-metal oxides of IL kind are e.g. known for iron¹⁸, nickel^{19,20} and copper^{21–23} compounds. Generally for late transition-metal oxides, the $\text{TM}(3d)$ subshell of $t_{2g} = \{d_{xz}, d_{yz}, d_{xy}\}$ character is completely filled and orbitals from the $e_g = \{d_{z^2}, d_{x^2-y^2}\}$ sector are partially filled. Whereas most cuprates are prototypical charge-transfer insulators with a comparatively small charge gap, many nickelates also carry substantial Mott-Hubbard character. Furthermore, while IL cuprates host the common formal Cu^{2+} oxidation state, as the perovskite compounds, IL nickelates formally host the uncommon Ni^+ oxidation state²⁴, when Ni^{2+} is usually realized in other nickel oxides. Thus one expects crucial normal-state differences between IL cuprates and nickelates at stoichiometry and with finite doping, largely effecting also the superconducting instability.

In this paper, we focus on a qualitative comparison of the long-known cuprate SrCuO_2 with the isostructural nickelate NdNiO_2 . The former compound is a charge-transfer insulator²⁵ and becomes a high-temperature superconductor upon doping and further alloying^{22,23}. On the other hand, the measured conductivity³ in the stoichiometric IL nickelate does not suggest a sizable charge gap. Our realistic many-body study takes care of the subtle interplay between charge-transfer and Mott-Hubbard physics in these late TM oxides. Full charge self-consistency and full rotational invariance in the lo-

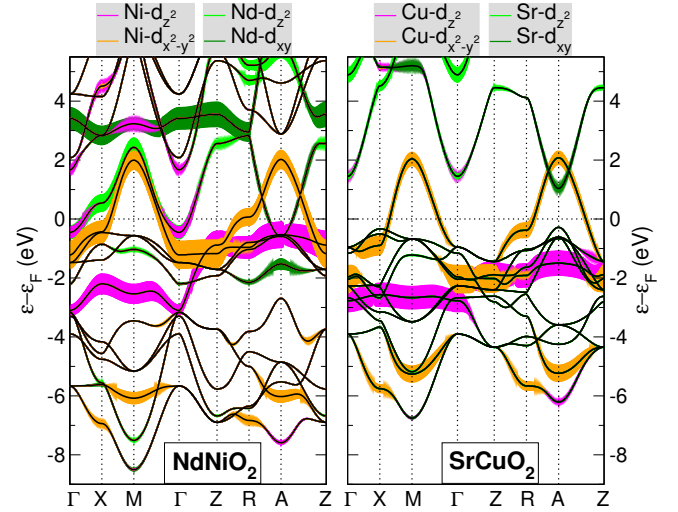


FIG. 1. (color online) DFT band structure of NdNiO_2 (left) and SrCuO_2 (right) along high-symmetry lines in the Brillouin zone. Color coded are the dominant orbital weights $\text{Ni-}d_{z^2}$, $\text{Ni-}d_{x^2-y^2}$ and $\text{Nd-}d_{z^2}$, $\text{Nd-}d_{xy}$ as well as $\text{Cu-}d_{z^2}$, $\text{Cu-}d_{x^2-y^2}$ and $\text{Sr-}d_{z^2}$, $\text{Sr-}d_{xy}$ close to the Fermi level.

cal $\text{TM}(3d)$ Coulomb interaction is combined with the inclusion of electron correlations stemming from oxygen sites. Important differences between both compounds, and points for NdNiO_2 toward a coexistence of Mott-critical layers with residual metallicity due to a subtle coupling between NiO_2 and Nd sheets. Upon hole doping, the stronger multi-orbital Mott-Hubbard character of the nickelate at low energy becomes evident, different from the Zhang-Rice physics of the effective one-orbital cuprate.

Theoretical approach.— We employ the charge self-consistent combination²⁶ of density functional theory (DFT), self-interaction correction (SIC) and dynamical mean-field theory (DMFT) in the DFT+sicDMFT framework²⁷. There, TM sites of Ni or Cu chemical entity act as DMFT impurities and Coulomb interactions on O enter within SIC on the pseudopotential level²⁸. The DFT part consists of a mixed-basis pseudopotential code^{29–31} and the SIC is applied to the $2s$ and the $2p$ orbitals of oxy-

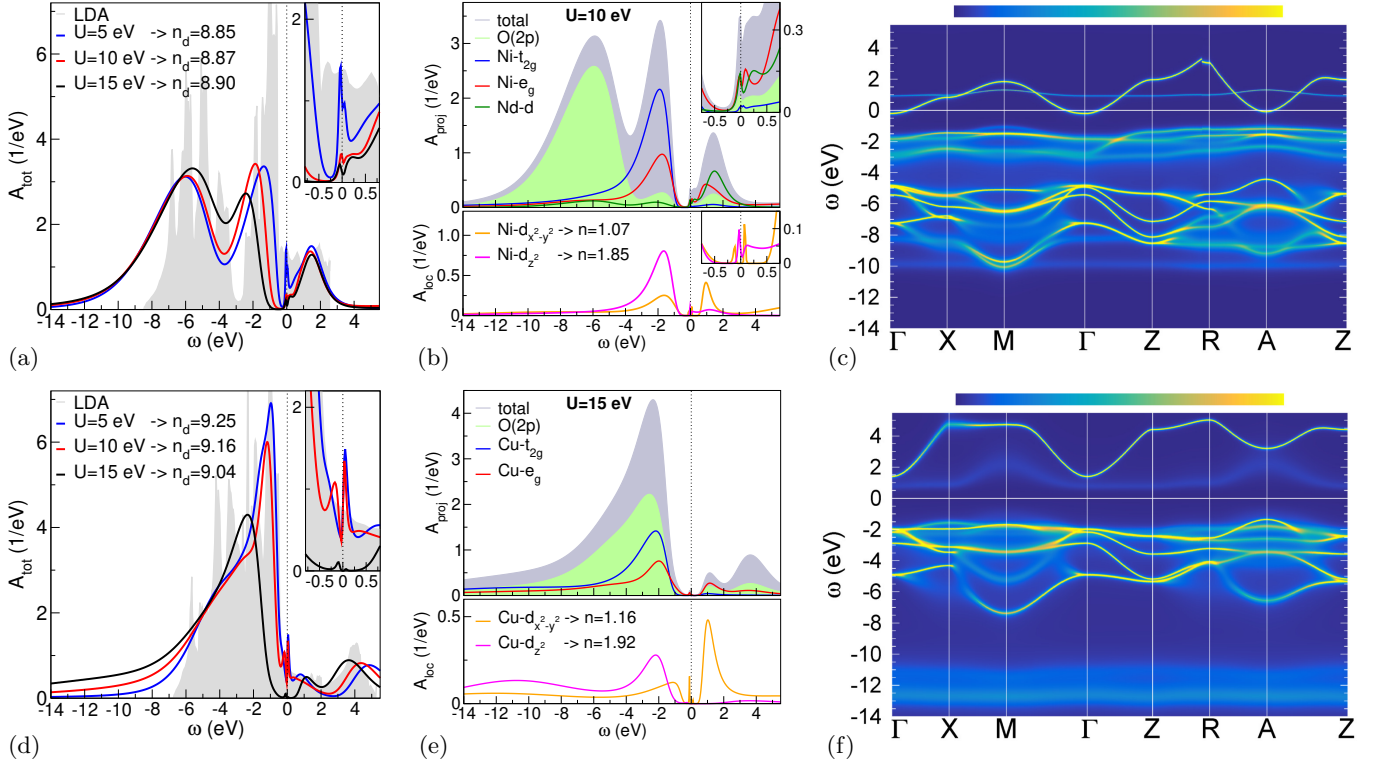


FIG. 2. (color online) DFT+sicDMFT spectral data of NdNiO₂ (top,a-c) and SrCuO₂ (bottom,d-f). (a,d) Total spectral function for $U = 5, 10, 15$ eV (insets: low-energy blow up) joint with the TM(3d) occupation n_d . (b,e) orbital- and site-projected spectral functions (upper part), and local TM- e_g spectral functions (lower part) joint with respective fillings n . (c,f) \mathbf{k} -resolved spectral function $A(\mathbf{k}, \omega)$ along high-symmetry lines. (b,c) are based on $U = 10$ eV and (e,f) on $U = 15$ eV.

gen via weight factors w_p (see Ref. 28 for more details). While the O(2s) orbital is by default fully corrected with $w_p = 1.0$, the common choice^{27,28} $w_p = 0.8$ is used for O(2p) orbitals. Note that we put the Nd(4f) states in the pseudopotential core. Continuous-time quantum Monte Carlo in hybridization expansion³² as implemented in the TRIQS code^{33,34} is utilized to solve the DMFT problem. In the DMFT correlated subspace, a five-orbital full Slater-Hamiltonian is applied to the TM projected-local orbitals³⁵. The fully-localized double-counting scheme³⁶ is applied. All many-body calculations are performed in the paramagnetic regime for the system temperature $T = 193$ K. Maximum-entropy and Padé methods are employed for the analytical continuation from Matsubara space onto the real-frequency axis. Stoichiometric lattice parameters are overtaken from experiment^{3,22}.

Stoichiometric case.— Figure 1 displays the nonmagnetic DFT band structures based on the local density approximation (LDA) for NdNiO₂ and SrCuO₂. Generally, the TM(3d) levels are closest to the Fermi level ε_F , while the dominant part of O(2p) lies deeper in energy. The oxygen 2p levels are much more intertwined with TM(3d) in the cuprate, pointing to a stronger charge-transfer character of SrCuO₂. We estimate the charge-transfer energy from $\Delta = \varepsilon_d - \varepsilon_p$, where ε_d and ε_p amount to the average energy of the TM(3d) and O(2p) level as computed in DFT+SIC²⁷. This re-

sults in $\Delta_{\text{NdNiO}_2} = 5.0$ eV and an indeed much lower $\Delta_{\text{SrCuO}_2} = 1.3$ eV. Similar calculations for rocksalt NiO resulted in $\Delta_{\text{NiO}} = 4.5$ eV²⁷. While SrCuO₂ displays a single-sheet Fermi surface of dominant Cu- $d_{x^2-y^2}$ character, a second band crosses ε_F in NdNiO₂, giving rise to electron pockets at Γ and A. In both compounds, the Fermi sheets overall enclose a volume corresponding to one electron. The additional weakly-filled band in the nickelate has mixed character of mainly Nd- d_{z^2} and Ni- d_{z^2} around Γ as well as of Nd- d_{xy} and Ni- d_{xz} , Ni- d_{yz} around A. It marks the self-doped nature of the IL nickelate. Similar hybridizations around Γ and A may also be observed in the cuprate case, along with the parallel contributions of Sr- d_{z^2} and Sr- d_{xy} . However there, the corresponding band above the dominant Cu- $d_{x^2-y^2}$ dispersion does not cross the Fermi level. The Ni- e_g based nearest-neighbor hoppings t to Nd- $d_{z^2,xy}$, as extracted in a wide-energy picture from the Wannier-like projected-local-orbital formalism³⁵, read $t_{\text{Ni}-d_{z^2}}^{\text{Nd}-d_{z^2}} = 18$ meV and $t_{\text{Ni}-d_{z^2}}^{\text{Nd}-d_{xy}} = -69$ meV. Such hoppings between Ni- $d_{x^2-y^2}$ and Nd- $d_{z^2,xy}$ are zero. The additional low-energy relevance of Ni- d_{z^2} from the e_g sector in IL nickelates has already been emphasized by Lee and Pickett²⁴. Note that the TM(4s) level hybridizes over a large energy range (not explicitly displayed), with appreciable weight in the O(2p)-block bottom, close to ε_F and well above the Fermi

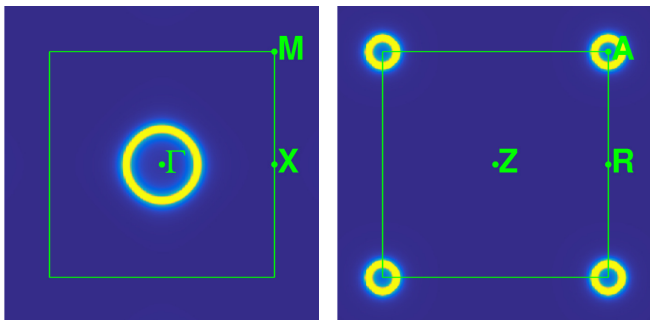


FIG. 3. (color online) Interacting ($U = 10$ eV) Fermi surface of NdNiO₂ in the $k_z = 0$ (left) and the $k_z = 0.5$ (right) plane of the Brillouin zone (green square) at $T = 193$ K.

level. It does not play a relevant role for the encountered nickelate fermiology.

For the realistic many-body description beyond LDA, we take up a pragmatic position concerning the local Coulomb parameters. In late TM oxides, a value $J_H = 1$ eV is a common choice for the Hund's exchange. For the better-screened Hubbard U , a value of 10 eV recently provided very good agreement between theory and experiment for stoichiometric as well as Li-doped NiO within DFT+*sicDMFT*²⁷. While some authors expect a smaller U in IL nickelate, the value for cuprates is usually expected larger than for nickelates. Hence, we start with the three different values $U = 5, 10, 15$ eV to cover the principally possible interaction space.

Figures 2a,d show the total \mathbf{k} -integrated spectral function from DFT+*sicDMFT* using the three different U values for NdNiO₂ and SrCuO₂. The $O(2p)$ block is shifted to deeper energies by ~ 1 eV for the former compound, due to the underestimation of the charge-transfer energy Δ within LDA. As expected, the cuprate compound becomes insulating at large U with a gap of about 1.5 eV, i.e. on the order of Δ . For the present largest choice of U , there is still some minor in-gap weight close to zero energy. A large value of $U > 10$ eV is not unreasonable in extended DMFT schemes for cuprates³⁷, yet antiferromagnetic ordering surely additionally supports gap opening. The nickelate compound avoids an insulating state even for $U = 15$ eV, i.e. the self-doped character remains robust up to large interaction strengths. Notably, the TM- $d_{x^2-y^2}$ weight is essentially gapped for NdNiO₂ at $U = 10$ eV and for SrCuO₂ at $U = 15$ eV, which from that viewpoint renders the nickelate more strongly correlated. The TM($3d$) occupation n_d approaches the formal d^9 value in both cases with growing U . To proceed with further details, we narrow down the range of U values to a single one for each compound via comparison to experiment: SrCuO₂ is a verified charge-transfer insulator, thus $U = 15$ eV is chosen; NdNiO₂ appears only weakly conducting, therefore we discard $U = 5$ eV, and stick to $U = 10$ eV as a well-established value for nickelates. For the rest of the paper, these two choices should ensure a qualitatively reliable comparison of the correlated elec-

tronic structure of both compounds.

The orbital- and site projected spectral functions in Figs. 2b,e underline the different $O(2p)$ position in the nickelate and the cuprate. In the case of SrCuO₂, the lower Hubbard band (around -12 eV) lies well below $O(2p)$, whereas for NdNiO₂ (around -9 eV) it is located in the deeper-energy part of $O(2p)$. Both materials display sizable charge-transfer character, but with much stronger fingerprint in SrCuO₂. The charge-transfer signature in NdNiO₂ is weaker as e.g. in NiO²⁷. Both TM- e_g contributions, i.e. $x^2 - y^2$ and z^2 , are gapped for SrCuO₂, while the z^2 character takes part in the self-doped state, along with Nd($5d$), in the case of the nickelate. At $U = 10$ eV, the $x^2 - y^2$ orbital in NdNiO₂ still marks contributions at lower energy, which are finally completely gone for $U = 15$ eV. The e_g occupations show that Ni- d_{z^2} is indeed further away from complete filling than Cu- d_{z^2} , and hence more susceptible to charge fluctuations. Thus, a novel variant of orbital selectivity emerges, with localized Ni- $d_{x^2-y^2}$ and weakly-itinerant Ni- d_{z^2} thanks to hybridization with Nd($5d$) in a self-doped manner. Though coupling between localized and itinerant electrons via e.g. inter-orbital effects on Ni is evident, a straightforward Kondo picture in terms of Nd- $d_{z^2,xy}$ allying with localized Ni- $d_{x^2-y^2}$ does seemingly not apply. The \mathbf{k} -resolved spectral functions in Figs. 2c,f confirm the previous statements on cuprate gap, nickelate self doping, and TM($3d$) vs. $O(2p)$ position. Furthermore, in the NdNiO₂ case the dd -coupling of Ni- e_g to Nd is favored for the self-doping band: compared to the LDA result which locates the electron pocket at A deeper in energy, the many-body calculation intensifies the stronger Ni- d_{z^2} -to-Nd- d_{z^2} hybridized electron pocket at Γ . Finally, the plotted nickelate Fermi surface in Fig. 3 displays circular sheets around Γ and A corresponding to the electron pockets of the self-doping band. Note again that the spectral weight of the hole band of mainly Ni- $d_{x^2-y^2}$ character is fully transferred to Hubbard bands at the given interaction strength due to the specific orbital-selective Mott transition in NdNiO₂.

Hole-doped case.— Let us turn to the electronic states with hole doping. The doped cases are realized by $2 \times 2 \times 2$ supercells of the nickelate and cuprate unit cells, respectively. This amounts to eight TM sites in the primitive cell, compared to only one in the stoichiometric unit cell. In the nickelate, Nd atoms are replaced by Sr atoms³ by a fraction x , while in the cuprate, Sr vacancies²⁵ are generated by a fraction y . For Nd_{1-x}Sr_xNiO₂, two supercells are constructed: replacing one Nd atom ($x = 0.125$), and replacing two Nd atoms ($x = 0.250$). For Sr_yCuO₂, one vacant Sr site is introduced ($y = 0.125$). Structural relaxation of the atomic positions within DFT+ U leads to a minor modulation of mainly the TM-O bond lengths, up to 0.5% of the respective stoichiometric distances. Notably, since each Sr vacancy gives rise to two holes, the actual doping level δ amounts to $\delta = x = 2y$. Note also again that we are here interested in principle effects and differences, and a very thorough many-body study of late

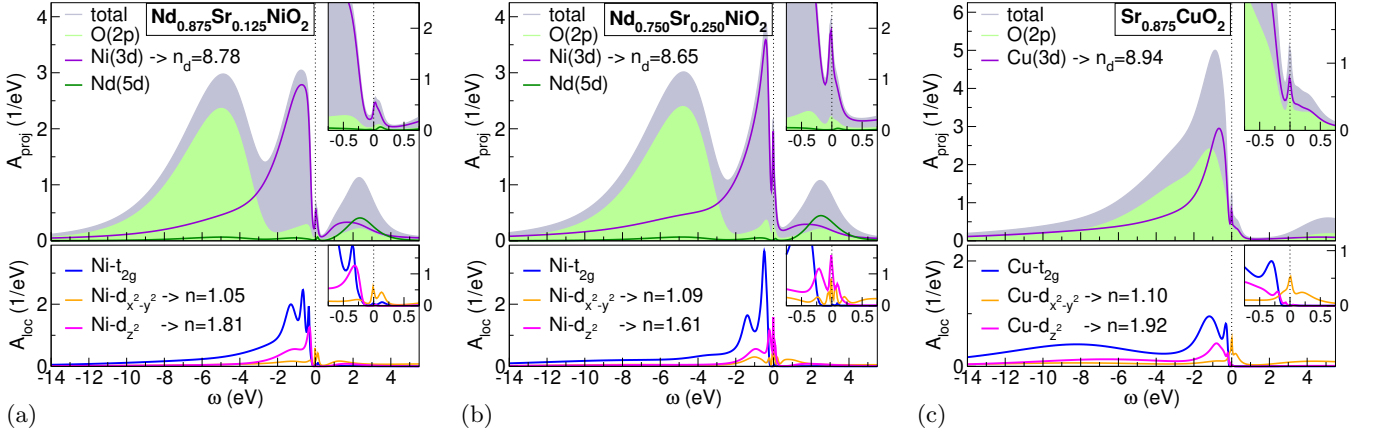


FIG. 4. (color online) DFT+sicDMFT spectral data of hole-doped materials. Upper parts: total as well as site- and orbital-projected spectral function (inset: low-energy blow up), with filling n_d of the TM(3d) shell. Lower parts: TM(3d) local spectral function, with filling n of the e_g orbitals. (a) $\text{Nd}_{0.875}\text{Sr}_{0.125}\text{NiO}_2$, (b) $\text{Nd}_{0.750}\text{Sr}_{0.250}\text{NiO}_2$ and (c) $\text{Sr}_{0.875}\text{CuO}_2$.

quasi-two-dimensional TM oxides at finite doping will ask for correlation effects beyond single-site DMFT (see e.g. Refs. 38 and 39 for reviews).

Figure 4 displays the spectral properties of the three hole-doping scenarios. In all cases, the electronic spectrum is shifted upwards in energy with doping, in line with available experimental data for IL cuprates^{25,40}. The doped charge-transfer insulator shows in Fig. 4c the spectral signature expected from a hole-doped cuprate⁴⁰: filling of the gap and a resonance at ε_F , both with a substantial contribution from O(2p) states. Comparing the occupation numbers, $\delta_{\text{Cu}} = n_d^{\text{undoped}} - n_d^{\text{doped}} = 0.10$ holes per site are located on copper, while $\delta_{\text{O}} = \delta - \delta_{\text{Cu}} = 0.15$ holes per site are attributed to oxygen. The low-energy resonance marks the itinerant Zhang-Rice singlet physics⁴¹. Hence, on the local Cu(3d) level, only the $x^2 - y^2$ orbital is contributing to the low-energy resonance. The situation is more intriguing for $\text{Nd}_{1-x}\text{Sr}_x\text{NiO}_2$ (cf. Fig. 4a,b). First, significant low-energy Zhang-Rice physics cannot readily be identified, the spectrum close to ε_F is strongly Ni(3d) dominated. Comparing the occupation numbers as before, a much larger relative hole count of $\delta_{\text{Ni}} = 0.09$ for $x = 0.125$ and of $\delta_{\text{Ni}} = 0.22$ for $x = 0.250$ on the TM site is obtained. Second, while for $x = 0.125$ the $x^2 - y^2$ orbital is mainly susceptible to doping, for $x = 0.250$ the z^2 orbital joins in^{10,15} and takes over. Because of the missing Zhang-Rice physics, holes are not easily shared between Ni and O sites. Thus for larger hole content, the Ni site has to provide access to additional orbital degrees of freedom. This would result in a $x^2 - y^2$ vs. z^2 multi-orbital competition at the experimental $x = 0.2$ scenario for superconductivity³. The prominent z^2 role is also supported by the favorable hybridizations established at stoichiometry. Note that the self-doping band itself is depleted already for the given dopings. While some minor Nd spectral content may still be observed at low energy, the actual electron pockets are shifted upwards by ~ 0.9 eV

for $x = 0.125$.

Summary and discussion.— There are key differences between the infinite-layer TM oxides NdNiO_2 and SrCuO_2 . The cuprate is a charge-transfer insulator at strong coupling, whereas the nickelate remains a non-insulating, self-doped system at large interaction strength. Still, in both system the TM- $d_{x^2-y^2}$ state is half-filled localized (or very close to such a regime). In the IL architecture it is naturally expected that the missing apical oxygens allow for novel/modified hybridization scenarios for the TM(3d) orbitals with the surrounding. In the cuprate case, this does not lead to major qualitative changes compared to the perovskite case, since hybridization with non-oxygen orbitals leads to states too high in energy to effect low-energy properties. On the other hand for rare-earth nickelates, the 5d orbitals of the rare-earth ion enable low-energy hybridization with Ni(3d), i.e. additional band crossing at ε_F from self doping. The Fermi surface becomes multi-sheeted, but still encompassing one electron. At strong coupling, where experiment seemingly places the material³, the $d_{x^2-y^2}$ dominated sheet becomes gapped, but Luttinger theorem ensures the survival of the self-doping sheet.

For hole doping, the role of the self-doping band becomes minor for sizable dopings. However, a strong TM(3d)-O(2p) coupling at low energy is absent for the nickelate, and furthermore, $x^2 - y^2$ and z^2 compete close to the Fermi level. On the other hand, hole-doped SrCuO_2 displays the expected $x^2 - y^2$ dominance even for the present overdoped scenario in view of superconductivity. One may speculate if the reduced T_c for the nickelate compared to cuprates may be the result of that competition. For instance, due to loss of coherence in the interplay between two rather differently characterized orbital settings. The effective single-TM(3d) orbital together with the strong Zhang-Rice physics would then be key to the high T_c of cuprates.

Further studies on IL nickelates and akin systems are highly desirable to fathom the designing options in view

of raising T_c ¹². In this context, the route along the metal-insulator transition in the oxygen-deficient LaNiO_{3-x} perovskite for $x \geq 0.25$ with apparent oxygen-vacancy ordering is also noteworthy^{42–44}.

ACKNOWLEDGMENTS

The author thanks A. J. Millis and R. Valentí for helpful discussions. Financial support from the German Science Foundation (DFG) via the project LE-2446/4-1 is gratefully acknowledged. Computations were performed at the University of Hamburg and the JUWELS Cluster of the Jülich Supercomputing Centre (JSC) under project number hhh08.

- ¹ J. Zaanen, G. A. Sawatzky, and J. W. Allen, Phys. Rev. Lett. **55**, 418 (1985).
- ² J. G. Bednorz and K. A. Müller, Z. Physik B - Condensed Matter **64**, 189 (1986).
- ³ D. Li, K. Lee, B. Y. Wang, M. Osada, S. Crossley, H. R. Lee, Y. Cui, Y. Hikita, and H. Hwang, Nature **572**, 624 (2019).
- ⁴ Q. Li, C. He, J. Si, X. Zhu, Y. Zhang, and H.-H. Wen, arXiv:1911.02420 (2019).
- ⁵ X. Zhou, Z. Feng, P. Qin, H. Yan, S. Hu, H. Guo, X. Wang, H. Wu, X. Zhang, H. Chen, et al., arXiv:1911.04662 (2019).
- ⁶ Y. Gu, S. Zhu, X. Wang, J. Hu, and H. Chen, arXiv:1911.00814 (2019).
- ⁷ M. Hepting, D. Li, C. J. Jia, H. Lu, E. Paris, Y. Tseng, X. Feng, M. Osada, E. Been, Y. Hikita, et al., Nat. Mater. doi:10.1038/s41563-019-0585-z (2020).
- ⁸ L.-H. Hu and C. Wu, Phys. Rev. Research **1**, 032046 (2019).
- ⁹ J. Hirsch and F. Marsiglio, Physica C: Superconductivity and its Applications **566**, 1353534 (2019).
- ¹⁰ M. Jiang, M. Berciu, and G. A. Sawatzky, arXiv:1909.02557 (2019).
- ¹¹ P. Jiang, L. Si, Z. Liao, and Z. Zhong, Phys. Rev. B **100**, 201106 (2019).
- ¹² Y. Nomura, M. Hirayama, T. Tadano, Y. Yoshimoto, K. Nakamura, and R. Arita, Phys. Rev. B **100**, 205138 (2019).
- ¹³ S. Ryee, H. Yoon, T. J. Kim, M. Y. Jeong, and M. J. Han, Phys. Rev. B **101**, 064513 (2020).
- ¹⁴ L. Si, W. Xiao, J. Kaufmann, J. M. Tomczak, Y. Lu, Z. Zhong, and K. Held, arXiv:1911.06917 (2019).
- ¹⁵ P. Werner and S. Hoshino, Phys. Rev. B **101**, 041104(R) (2020).
- ¹⁶ X. Wu, D. D. Sante, T. Schwemmer, W. Hanke, H. Y. Hwang, S. Raghu, and R. Thomale, Phys. Rev. B **101**, 060504(R) (2020).
- ¹⁷ G.-M. Zhang, Y.-F. Yang, and F.-C. Zhang, Phys. Rev. B **101**, 020501(R) (2020).
- ¹⁸ Y. Tsujimoto, C. Tassel, N. Hayashi, T. Watanabe, H. K. K. Yoshimura, M. Takano, M. Ceretti, C. Ritter, and W. Paulus, Nature **450**, 1062 (2007).
- ¹⁹ M. Crespín, P. Levitz, and L. Gatineau, J. Chem. Soc., Faraday Trans. 2 **79**, 1181 (1983).
- ²⁰ M. A. Hayward and M. J. Rosseinsky, Solid State Sci. **5**, 839 (2003).
- ²¹ T. Siegrist, S. M. Zahurak, D. W. Murphy, and R. S. Roth, Nature **334**, 231 (1988).
- ²² M. G. Smith, A. Manthiram, J. Zhou, J. B. Goodenough, and J. T. Markert, Nature **351**, 549 (1991).
- ²³ M. Azuma, Z. Hiroi, M. Takano, Y. Bando, and Y. Takeda, Nature **356**, 775 (1992).
- ²⁴ K.-W. Lee and W. E. Pickett, Phys. Rev. B **70**, 165109 (2004).
- ²⁵ N. Terada, A. Iyo, Y. Sekita, S. Ishibashi, and H. Ihara, Czech. J. Phys. **46**(Suppl 5), 2683 (1996).
- N. Terada, S. Ishibashi, M. Jo, M. Hirabayashi, and H. Ihara, J. Phys. Chem. Solids **54**, 1207 (1993).
- ²⁶ D. Grieger, C. Piefke, O. E. Peil, and F. Lechermann, Phys. Rev. B **86**, 155121 (2012).
- ²⁷ F. Lechermann, W. Körner, D. F. Urban, and C. Elsässer, Phys. Rev. B **100**, 115125 (2019).
- ²⁸ W. Körner and C. Elsässer, Phys. Rev. B **81**, 085324 (2010).
- ²⁹ C. Elsässer, N. Takeuchi, K. M. Ho, C. T. Chan, P. Braun, and M. Fahnle, J. Phys.: Condens. Matter **2**, 4371 (1990).
- ³⁰ F. Lechermann, F. Welsch, C. Elsässer, C. Ederer, M. Fahnle, J. M. Sanchez, and B. Meyer, Phys. Rev. B **65**, 132104 (2002).
- ³¹ B. Meyer, C. Elsässer, F. Lechermann, and M. Fahnle, *FORTRAN 90 Program for Mixed-Basis-Pseudopotential Calculations for Crystals*, Max-Planck-Institut für Metallforschung, Stuttgart (1998).
- ³² P. Werner, A. Comanac, L. de' Medici, M. Troyer, and A. J. Millis, Phys. Rev. Lett. **97**, 076405 (2006).
- ³³ O. Parcollet, M. Ferrero, T. Ayral, H. Hafermann, I. Krivenko, L. Messio, and P. Seth, Comput. Phys. Commun. **196**, 398 (2015).
- ³⁴ P. Seth, I. Krivenko, M. Ferrero, and O. Parcollet, Comput. Phys. Commun. **200**, 274 (2016).
- ³⁵ B. Amadon, F. Lechermann, A. Georges, F. Jollet, T. O. Wehling, and A. I. Lichtenstein, Phys. Rev. B **77**, 205112 (2008).
- ³⁶ V. I. Anisimov, I. V. Solovyev, M. A. Korotin, M. T. Czyżyk, and G. A. Sawatzky, Phys. Rev. B **48**, 16929 (1993).
- ³⁷ S. Choi, A. Kutepov, K. Haule, M. van Schilfgaarde, and G. Kotliar, npj Quantum Materials **1**, 16001 (2016).
- ³⁸ T. Maier, M. Jarrell, T. Pruschke, and M. H. Hettler, Rev. Mod. Phys. **77**, 1027 (2005).
- ³⁹ G. Rohringer, H. Hafermann, A. Toschi, A. A. Katanin, A. E. Antipov, M. I. Katsnelson, A. I. Lichtenstein, A. N. Rubtsov, and K. Held, Rev. Mod. Phys. **90**, 025003 (2018).
- ⁴⁰ C. T. Chen, F. Sette, Y. Ma, M. S. Hybertsen, E. B. Stechel, W. M. C. Foulkes, M. Schultze, S.-W. Cheong, A. S. Cooper, L. W. Rupp, et al., Phys. Rev. Lett. **66**, 104 (1991).
- ⁴¹ F. C. Zhang and T. M. Rice, Phys. Rev. B **37**, 3759(R) (1988).

- ⁴² M. J. Sayagués, M. Vallet-Regí, A. Caneiro, and J. M. González-Calbet, *J. Solid State Chem.* **110**, 295 (1994).
- ⁴³ R. D. Sánchez, M. T. Causa, A. Caneiro, A. Butera, M. Vallet-Regí, M. J. Sayagués, J. González-Calbet, F. García-Sanz, and J. Rivas, *Phys. Rev. B* **54**, 16574 (1996).
- ⁴⁴ B.-X. Wang, S. Rosenkranz, X. Rui, J. Zhang, F. Ye, H. Zheng, R. F. Klie, J. F. Mitchell, and D. Phelan, *Phys. Rev. Materials* **2**, 064404 (2018).